European Journal of Cancer 146 (2021) 11–20

Available online at www.sciencedirect.com

ScienceDirect

journal homepage: www.ejcancer.com

Original Research

A multimodal molecular imaging approach targeting urokinase plasminogen activator receptor for the diagnosis, resection and surveillance of urothelial cell carcinoma

Victor M. Baart [a,*], Geertje van der Horst [b], Marion M. Deken [a], Shadhvi S. Bhairosingh [a], Timo Schomann [c,d], Vincent Q. Sier [a], Maaike H. van der Mark [b], Luisa Iamele [e], Hugo de Jonge [e], Massimo Resnati [f], Andrew P. Mazar [g], Rob C.M. Pelger [b], Gabriel van der Pluijm [b], Peter J.K. Kuppen [a], Alexander L. Vahrmeijer [a], Cornelis F.M. Sier [a,d]

[a] *Department of Surgery, Leiden University Medical Centre, Leiden, the Netherlands*
[b] *Department of Urology, Leiden University Medical Centre, Leiden, the Netherlands*
[c] *Department of Radiology, Leiden University Medical Centre, Leiden, the Netherlands*
[d] *Percuros BV, Leiden, the Netherlands*
[e] *Department of Molecular Medicine, Immunology and General Pathology Unit, University of Pavia, Pavia, Italy*
[f] *Age Related Diseases Unit, Division of Genetics and Cell Biology, San Raffaele Scientific Institute, Milano, Italy*
[g] *Monopar Therapeutics, Wilmette, IL, USA*

Received 6 November 2020; received in revised form 22 December 2020; accepted 7 January 2021
Available online 6 February 2021

KEYWORDS
Image guided surgery;
Photoacoustic imaging;
EpCAM;

Abstract With a 5-year recurrence rate of 30–78%, urothelial cell carcinoma (UCC) rates amongst the highest of all solid malignancies. Consequently, after transurethral resection, patients are subjugated to life-long endoscopic surveillance. A multimodal near-infrared (NIR) fluorescence-based imaging strategy can improve diagnosis, resection and surveillance, hence increasing quality of life.

Abbreviations: EpCAM, Epithelial cell adhesion molecule; EV, Empty vector; IHC, Immunohistochemistry; LUMC, Leiden University Medical centre; MFIs, Mean fluorescence intensities; MIBC, Muscle invasive bladder cancer; NIR, Near-infrared; NMIBC, Non-muscle invasive bladder cancer; PA, Photoacoustic; PpIX, Protoporphyrin; TBR, Tumour-to-background ratio; TIS, Total immunostaining score; TNFα, Tumour necrosis factor alpha; TUR, Transurethral resection; UCC, Urothelial cell carcinoma; uPAR, Urokinase plasminogen activator receptor; WT, Wild-type; 5-ALA, 5-Aminolevulinic acid.

* *Corresponding author*: Department of Surgery, LUMC, Albinusdreef 2, 2333, ZA, Leiden, the Netherlands. Fax: +71 526 6750.
E-mail address: v.m.baart@lumc.nl (V.M. Baart).

https://doi.org/10.1016/j.ejca.2021.01.001

Bladder cancer;
Radical cystectomy;
Transurethral resection;
TUR surgery

Methods: Expression of urokinase plasminogen activator receptor (uPAR) and epithelial cell adhesion molecule (EpCAM) are determined on paraffin-embedded human UCC using immunohistochemistry and on UCC cell lines by flow cytometry. MNPR-101, a humanised monoclonal antibody targeting uPAR is conjugated to IRDye800CW and binding is validated *in vitro* using surface plasmon resonance and cell-based binding assays. *In vivo* NIR fluorescence and photoacoustic three-dimensional (3D) imaging are performed with subcutaneously growing human UM-UC-3luc2 cells in BALB/c-nude mice. The translational potential is confirmed in a metastasising UM-UC-3luc2 orthotopic mouse model. Infliximab-IRDye800CW and rituximab-IRDye800CW are used as controls.

Results: UCCs show prominent uPAR expression at the tumour-stroma interface and EpCAM on epithelial cells. uPAR and EpCAM are expressed by 6/7 and 4/7 UCC cell lines, respectively. *In vitro,* MNPR-101-IRDye800CW has a picomolar affinity for domain 2-3 of uPAR. *In vivo* fluorescence imaging with MNPR-101-IRDye800CW, specifically delineates both subcutaneous and orthotopic tumours with tumour-to-background ratios reaching as high as 6.8, differing significantly from controls ($p < 0.0001$). Photoacoustic 3D in depth imaging confirms the homogenous distribution of MNPR-101-IRDye800CW through the tumour.

Conclusions: MNPR-101-IRDye800CW is suitable for multimodal imaging of UCC, awaiting clinical translation.

1. Introduction

Despite advances in detection, treatment and surveillance of urothelial cell carcinoma (UCC), there has been no major improvement in overall prognosis over the past 30 years, with nearly 200,000 patients still succumbing annually [1,2]. Clinically, UCC represents two sequential entities: non-muscle invasive bladder cancer (NMIBC), where malignant cells are constrained to the epithelial layer, and muscle-invasive bladder cancer (MIBC) wherein the tumour invades surrounding subepithelial tissue [3]. The majority of UCC cases (75–85%) are NMIBC and are marked by a high 5-year recurrence rate of 30–78% and 7–40% chance of progression to MIBC disease after transurethral resection (TUR). Therefore, NMIBC requires intensive surveillance via cystoscopy [4,5]. Once UCC progresses, definitive therapy, defined as radical cystectomy with or without (neo)adjuvant therapy, is indicated [3]. Hereof, 6.3% show involved margins with significantly reduced recurrence-free and cancer-specific survival [6]. Consequentially, UCC causes a high burden of disease, where patients could benefit from improved TUR and tumour-free resection margins.

Real-time intraoperative guidance with near-infrared (NIR) fluorescence tracers has the potential to function as an extra sense, not only informing surgeons about tumour localisation during resection but also about the degree of disease-aggressiveness [7]. Fundamental for successful imaging is the identification of appropriate cancer-specific targets [8]. Ideally, a single target overexpressed in all patients (across multiple tumour types) is identified. Currently, no such target exists. Epithelial cell adhesion molecule (EpCAM) is one of the most promising pan-tumour targets, found to be overexpressed in most solid tumour types and is clinically being evaluated in NIR imaging studies (NL7363). UCC's, however, do not universally express EpCAM; 56% of UCCs are EpCAM negative and the overexpression rate compared with healthy tissue is 27% [9]. Hence, EpCAM-based tracers will not be applicable for all patients with UCC, requiring the search for alternative targets with complementary expression patterns.

An alternative candidate for UCC targeting is the urokinase plasminogen activator receptor (uPAR). uPAR narrowly orchestrates various tumour-specific processes, including cell differentiation, proliferation and migratio but is barely present in healthy tissues. Immunohistochemical localisation of uPAR on 186 human UCC specimens revealed expression of this receptor in 96% of the tumours, particularly at the invasive front, irrespective of grade and stage, while being completely absent in normal bladder [11]. Such a pattern is ideal for molecular imaging [12]. Recent preclinical studies confirmed the applicability of mouse anti-uPAR antibodies conjugated to the fluorophore ZW800-1 for optical imaging of oral and colorectal cancer [13,14]. However, the use of an alternative fluorophore, IRDye800CW (800F), offers the possibility of imaging via NIR light, as well as via photoacoustic (PA) imaging [8,15]. PA imaging uses the contrast of optical imaging with the spatial resolution of ultrasound, enabling a tissue penetration depth of several centimetres [15,16]. In the clinic, a bimodal tracer, capable of both optical NIR- and PA-imaging, can be used during non-invasive (transabdominal) surveillance, TURs, and radical cystectomies.

In this study, we developed a humanised NIR molecular imaging tracer for simultaneous fluorescence and PA-imaging to facilitate resection of human UCC in a clinically relevant mouse model.

2. Materials and methods

2.1. Human samples and immunohistochemistry

Formalin-fixed, paraffin-embedded tissue blocks of fourteen patients who underwent cystectomy or TUR for UCC were collected from the Department of Pathology of the Leiden University Medical Centre (LUMC). Sections of 4 μm were stained based on standard immunohistochemical (IHC) methods as described in Appendix A. Sections were digitalised using the Panoramic Digital Slide Scanner, viewed with Caseviewer 2.3 (both 3D Histech, Hungary) and scored for percentage of positive cells and staining intensity with the total-immunostaining score (TIS). TIS >4 was defined as overexpression [17]. The LUMC ethics review board approved the study protocol (B20.030). Samples and data were non-identifiable and used in accordance with the 1964 Helsinki declaration.

2.2. In silico analysis of gene expression in a TCGA data set

The freely available raw The Cancer Genome Atlas transcriptome database, consisting of bladder urothelial carcinoma samples (http://www.cbioportal.org/study?id=blca_tcga) was used to determine the correlation between the gene expression of EpCAM and uPAR/PLAUR in a mostly non-chemo-treated MIBC cohort of 408 patients.

2.3. Cells

Suppliers and culture conditions of the UCC cell lines UM-UC-3, J82, T24, RT112, RT4, HT-1197 and HT-1376, and the transfected cell lines HEK EV (empty vector), HEK uPAR wildtype (WT) and the cleaved isoform HEK uPAR D2-3 are described in Appendix B. Further characterisation of the UCC cells in accordance with patient characteristics and molecular profile can be found in Appendix C.1-2. Cell lines were routinely tested for mycoplasma.

2.4. Antibodies

ATN658 is an extensively validated mouse monoclonal antibody of the IgG1 κ isotype targeting domain 3 of uPAR [13,14]. MNPR-101 (formerly known as huATN658) is the humanised variant. Both antibodies are not cross-reactive with mouse uPAR [18]. Rituximab and infliximab (Remicade®) are clinical grade chimeric human-mouse antibodies, consisting of the glycosylated human IgG1 κ isotype constant domain, targeting CD20 and tumour necrosis factor-α (TNFα), respectively.

2.5. Surface plasmon resonance

Binding of ATN658 and MNPR-101(-800F) to recombinant human uPAR (10925-H08H, Sinobiological, China) was measured by surface plasmon resonance on a Biacore T200 instrument (GE Healthcare, USA) at 25 °C. uPAR was immobilised on a NiHC 1500 M chip (Xantec, Germany), and the interaction was measured at 2.5, 5, 10, 20, and 40 nM with four separate single-cycle kinetic experiments.

2.6. Cell-based assays

Quantitative flow cytometry using Qifi-kit (Agilent Technologies, USA) was performed based on suppliers instructions. Confluent chamber slides were incubated with primary antibodies, stained with fluorescein isothiocyanate-labelled secondary antibodies and 4′,6-diamidino-2-phenylindole, and imaged with a DM500 B microscope (Leica Microsystems, Germany). Binding of serially diluted fluorescence antibodies to cell-based plate assays were determined using the Odyssey CLx Imaging System (LI-COR Biosciences, USA). For detailed descriptions of these assays, see Appendix D.

2.7. Animal models

The Dutch Central Commission for Animal Experimentation approved all animal experiments (AVD1160020172925). Experiments were performed in accordance with the code of practice 'Dierproeven In Het Kankeronderzoek'. Each experimental group consisted of three-to-four 6-10-week-old female BALB/c-Nude mice (CAnN.Cg-*Foxn1*^{nu}/Crl, Charles River laboratories, France). Subcutaneous tumour models were induced by subcutaneous injection of 0.5×10^6 UM-UC-3luc2 cells (Appendix D). For the preclinical orthotopic xenograft model, luciferase-expressing UM-U3-luc2 cells were inoculated into the bladder as previously described [19].

2.8. In vivo NIRF imaging

Anaesthetised (1.5–4% isoflurane; Teva Pharmachemie BV, The Netherlands) mice were imaged with The Pearl Trilogy Small Animal Imaging System (LI-COR Biosciences, USA) and Artemis 1–7 days (Quest Medical Imaging, The Netherlands) 1–7 days after intravenous tracer injection. After sacrifice, tumours were resected, stained and scanned for 800 nm fluorescence using the Odyssey CLx Imaging System (LI-COR Biosciences, USA).

2.9. Photoacoustic imaging

Anaesthetised mice were immobilised on the preheated imaging table of the Vevo 3100 Imaging System (FUJIFILM VisualSonics, Canada) and covered with ultrasound gel. The Vevo 3100 Imaging System was equipped with a Vevo LAZR-X cart, a Vevo LAZR-Tight Enclosure, and a Vevo Imaging Station. For ultrasound and PA imaging, the MX550D transducer (25–55 MHz; Axial Resolution: 40 μm; excitation 780 nm) was used.

2.10. Image analyses and statistics

Tumour-to-background ratios (TBRs) were measured by drawing regions of interest around the tumour and the surrounding tissue, and dividing the mean fluorescence intensities (MFIs). In the orthotopic model, either fat or the caecum were used as background to determine tumour-to-organ ratios. For respective software, see Appendix D. Means, reported with standard deviations, were compared by two-way repeated measurement ANOVA with GraphPad Prism 8 (GraphPad Software, USA). Correlations are calculated based on Pearson and indicated by R^2. Significance levels are <0.05.

3. Results

3.1. EpCAM and uPAR are complementary targets for UCC

The IHC expression profiles of EpCAM and uPAR in UCC specimens were compared, as shown in Fig. 1A. Staining for EpCAM, when present, was homogenous throughout the tumour, resulting in a moderate to intense membrane staining of malignant cells. However, one-third of cases had no EpCAM expression. uPAR staining was most prominent at the tumour-stroma interface localising towards cancer cells and tumour-associated stromal cells, including macrophages (CD68 positive) and cancer-associated fibroblasts (aSMA) (Fig. 1B). Staining was moderate to strong in intensity at the cell membranes. Approximately two-thirds of tumour over expressed uPAR. EpCAM expression did not correlate with either epithelial uPAR ($R^2 = 0.20$, $p = 0.30$) or stromal uPAR ($R^2 = 0.21$, $p = 0.30$) with EpCAM, see also Figure Appendix E. All in all, 79% of patients overexpressed one or both targets. Expression patterns matched those seen in literature (Appendix F). In addition, mRNA expression levels of PLAUR and EpCAM on UCC tumour cells was independent of each other and confirmed their complementary nature ($p = 0.0059$, Figure Appendix G).

Table 1
Number of uPAR and EpCAM receptors per cell on UCC cell lines.

	uPAR	EpCAM
UM-UC-3luc2	20,000	n.d.
J82	84,000	n.d.
T24	7000	n.d.
RT112	25,000	139,000
RT4	n.d.	226,000
HT-1197	17,000	194,000
HT-1376	7000	64,000

n.d., not detectable, below detection limit.
UCC, urothelial cell carcinoma; uPAR, urokinase plasminogen activator receptor; EpCAM, epithelial cell adhesion molecule.

Using a panel of UCC cell lines, spanning the clinical range from NMIBC to MIBC, we assessed the number of copies for uPAR and EpCAM per cell. Six of seven cell lines expressed uPAR, ranging from 7000 to 84,000 copies per cell (Table 1). For EpCAM 4/7 cell lines were positive, ranging from 60,000–226,000. In summary, each cell line expressed either uPAR, EpCAM or both, with T24 as possibly problematic cell line, depending on only 7000 uPAR copies and none for EpCAM.

3.2. MNPR-101 targets domain 2-3 of uPAR with nanomolar affinities

Ideally, tracers for molecular imaging have a high affinity for all tumour-associated isoforms of the target. Humanisation of ATN658 into MNPR-101 did not alter the affinity for recombinant uPAR with a K_D for ATN658 of 0.5×10^{-9} M (K_a 1.6×10^5 M^{-s} s^{-1}; K_d

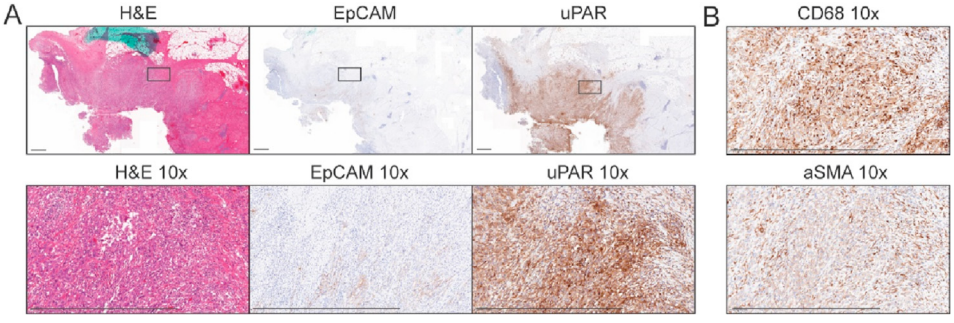

Fig. 1. UCC expression of uPAR and EpCAM. (A) Consecutive sections of a UCC case showing absent to weak EpCAM staining at the tumour borders and intense staining for uPAR in both tumour cells and tumour-associated stroma. (B) uPAR-positive stroma cells are, amongst others, CD68 positive macrophages and aSMA positive cancer associated fibroblasts. Black line = 1000 μm. Black box = insert. uPAR, urokinase plasminogen activator receptor; EpCAM, epithelial cell adhesion molecule.

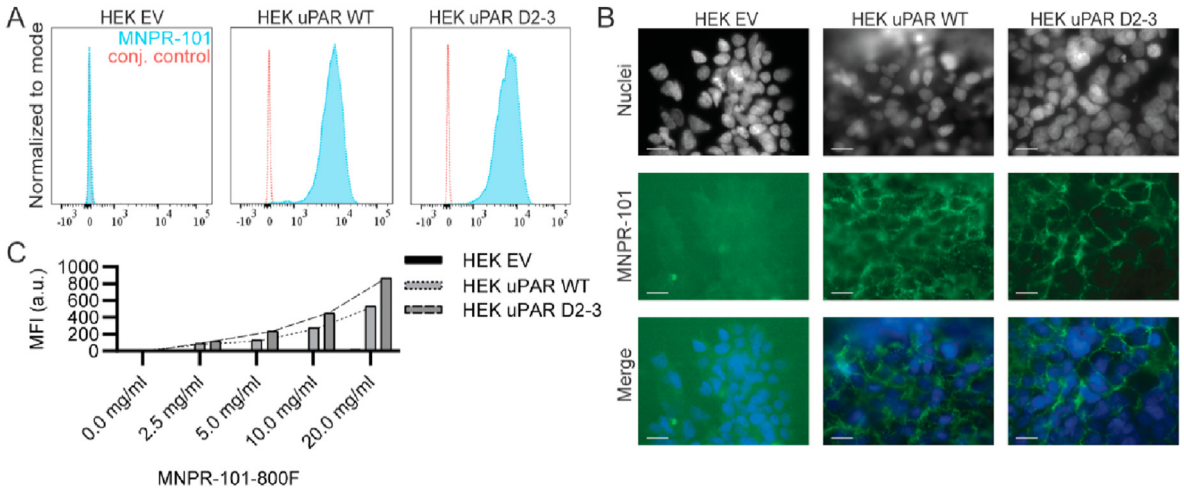

Fig. 2. *In vitro* validation of MNPR-101. (A) MNPR-101 binding per flow cytometry to empty vector (EV), wild-type (WT) and the cleaved isoform D2-3 transfected HEK cell lines. (B) Upon immunofluorescence microscopy binding could be seen to localise towards the cell membranes of WT and cleaved D2-3 transfected HEK cells but not EV transfected HEK cells. Green is MNPR-101 signal and grey/blue is a nuclear staining. Bar = 50 μm. (C) After conjugation to a near-infrared fluorescence dye, MNPR-101-800F demonstrated a concentration-dependent 800 nm signal increase on uPAR transfected HEK cells as measured using the Odyssey CLx. uPAR, urokinase plasminogen activator receptor. (For interpretation of the references to color in this figure legend, the reader is referred to the Web version of this article.)

7.0×10^{-5} s^{-1}) and MNPR-101 having a K_D of 0.2×10^{-9} M (K_a 3.6×10^5 M^{-1} s^{-1}; K_d 7.8×10^{-5} s^{-1}).

MNPR-101 binding was specific for the cell membranes of uPAR WT and D2-3 HEK cells but not HEK EV cells (Fig. 2A and B).

MNPR-101 was conjugated with 800F at a 1.1–1.5 labelling ratio, and was checked for unconjugated dye, as confirmed by respectively matrix assisted laser desorption ionization-time of flight mass spectrometry and sodium dodecyl sulfate polyacrylamide gel electrophoresis. Conjugation did not substantially affect the affinity of MNPR-101-800F for uPAR (K_D 0.3×10^{-9} M; K_a 6.1×10^5 M^{-1} s^{-1}; K_d 1.5×10^{-5} s^{-1}). A dose-dependent increase of 800 nm signal on cell-based plated assays with HEK uPAR WT and uPAR D2-3 cells, as well as constant low signal with HEK EV cells confirmed binding capacity (Fig. 2C).

3.3. NIR image-guided surgery of UCC with MNPR-101-800F

Fluorescence tracers can accumulate in tumours due to non-specific effects such as the enhanced-permeability and retention effect or blood pooling. To account for this effect, two non-cancer–related humanised monoclonal antibodies were used as non-specific controls. *In vitro,* MNPR-101 but not infliximab (anti-TNFα) or rituximab (anti-CD20) bound UM-UC-3luc2 cells (Fig. 3A).

The *in vivo* tumour recognition potential was subsequently assessed in mice bearing UM-UC-3luc2 subcutaneous tumours. Total mouse tumour burden did not differ significantly between experimental groups ($p = 0.6581$). After intravenous injection of 0.33 nmol, 1 nmol and 3 nmol MNPR-101-800F, mice were imaged daily with the preclinical Pearl and clinical Artemis imaging systems. Tumour MFI corresponded with the injected dose ($p < 0.0001$, Fig. 3B). TBRs did not differ significantly between dose groups with sufficient TBRs 3–7 days after imaging (Fig. 3C) and a TBR max of 2.9 five days after injection of 1 nmol MNPR-101-800F.

As specificity controls, subcutaneous UM-UC-3luc2 bearing mice were injected intravenously with 1 nmol infliximab-800F or rituximab-800F. TBRs differed significantly between MNPR-101-800F and the controls across all time points except for 4 h after injection ($p < 0.0001$, Fig. 3D). In contrast to infliximab-800F or rituximab-800F, tumours were readily visualised with the clinical Artemis system starting 3 days after MNPR-101-800F injection (Fig. 3D and E).

Intravesical injection of bioluminescent UM-UC-3luc2 cells into the murine bladder represents a preclinical orthotopic UCC model that allows optical imaging of cancer growth in real time [19]. Three weeks after tumour inoculation, 1 nmol MNPR-101-800F and rituximab-800F were injected intravenously and imaged three days later. Tumours where highly fluorescent after MNPR-101-800F injection matching bioluminescence signal and allowing image-guided resection (Fig. 4A, Appendix H). Importantly, *post-mortem* histology, fluorescence scanning and immunohistochemistry confirmed tumour cell specificity of MNPR-101-800F and only non-specific signal with rituximab-800F (Fig. 4B). MNPR-101-800F exhibited an average tumour-to-fat ratio of 2.6 (range: 2.3–3.2) and tumour-to-caecum ratios of 5.8 (range: 5.3–6.8) (Fig. 4C). The

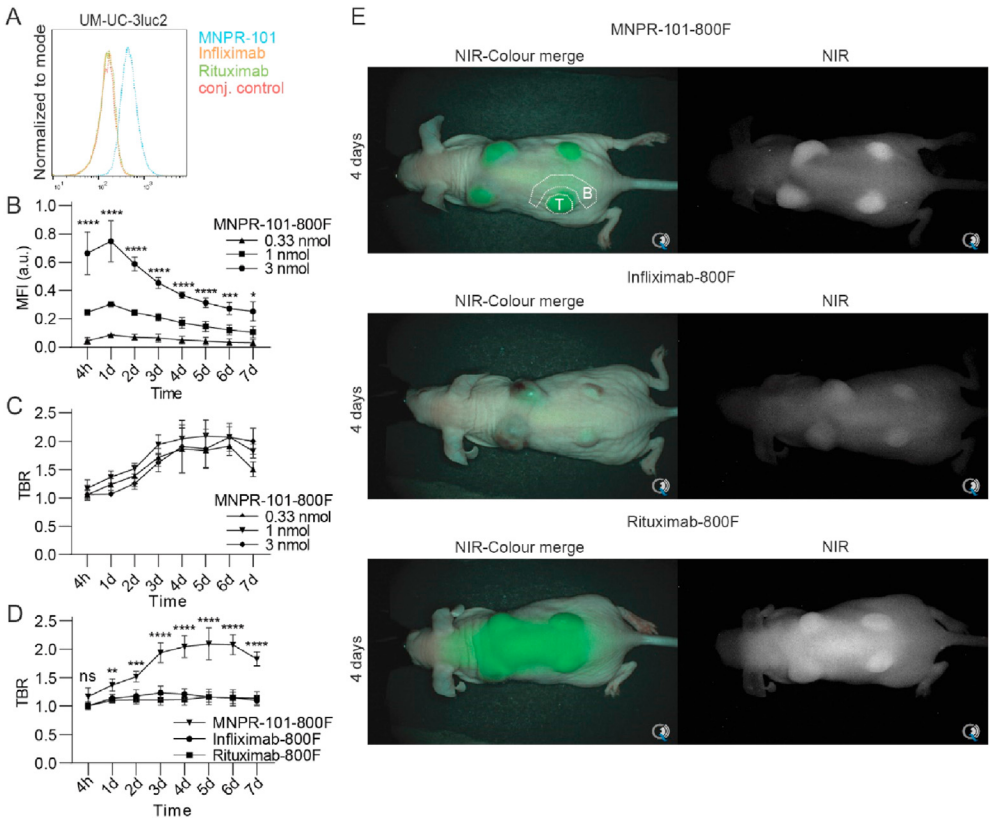

Fig. 3. NIR fluorescence imaging with MNPR-101-800F. (A) Flow cytometry of MNPR-101, infliximab and rituximab of UCC UM-UC-3luc2 cells. (B) *In vivo* tumour MFI's determined using the Pearl imaging system and (C) TBR's determined by the Artemis imaging system after intravenous injection of 0.33, 1 and 3 nmol MNPR-101-800F in subcutaneous UM-UC-3luc2 tumour-bearing mice. (D) *In vivo* TBRs determined by the Artemis imaging system after intravenous injection of 1 nmol MNPR-101-800F, infliximab-800F or rituximab-800F. (E) NIR-images of subcutaneous UM-UC-3luc2 bearing mice four days after administration of MNPR-101-800F, infliximab-800F and rituximab-800F. NIR images were taken with the clinical Artemis NIR-camera. A representative tumour (T) and background (B) region is shown. UCC, urothelial cell carcinoma; NIR, near-infrared; TBRs, tumour-to-background ratios; MFIs, mean fluorescence intensities.

tumour-to-fat ratio and tumour-to-caecum ratio for rituximab-800F were 1.3 and 3.2, respectively. On *post-mortem* biodistribution analysis of MNPR-101-800F, the majority of the fluorescence was seen in the tumour followed by the metabolising organs (Fig. 4D). The CD20 targeting rituximab-800F preferentially localised towards the liver and kidneys.

3.4. Photoacoustic imaging of UCC with MNPR-101-800F

The multimodal imaging potential of MNPR-101-800F was investigated by PA-imaging. Subcutaneous UM-UC-3luc2 tumour-bearing mice were injected intravenously with 3 nmol MNPR-101-800F and imaged three days after injection. High intensity signal was evident throughout the tumour and the skin while signal in surrounding structures remained minimal (Fig. 5A). Non-specific signal was noticed in the skin of phosphate-buffered saline-injected negative control mice (Fig. 5B).

4. Discussion

The recurring nature of UCCs and the tendency to progress are a significant burden for patients and health services [20,21]. Consequently, every effort should be made to improve therapy. Here, we implemented a novel approach that may facilitate and improve UCC detection and resection rates by intraoperative multimodal guidance using MNPR-101-800F.

The additional value of exogenous contrast agents during cystoscopy has already been demonstrated with 5-aminolevulinic acid (5-ALA) and its fluorescence metabolite protoporphyrin IX (PpIX) [22]. Using 5-ALA, 7–30% more UCCs were detected, residual tumour rate reduced by 20%, and cancer-free survival increased. However, the fluorescence properties of PpIX (excitation 375–440 nm, emission 635, 704 nm) are poor

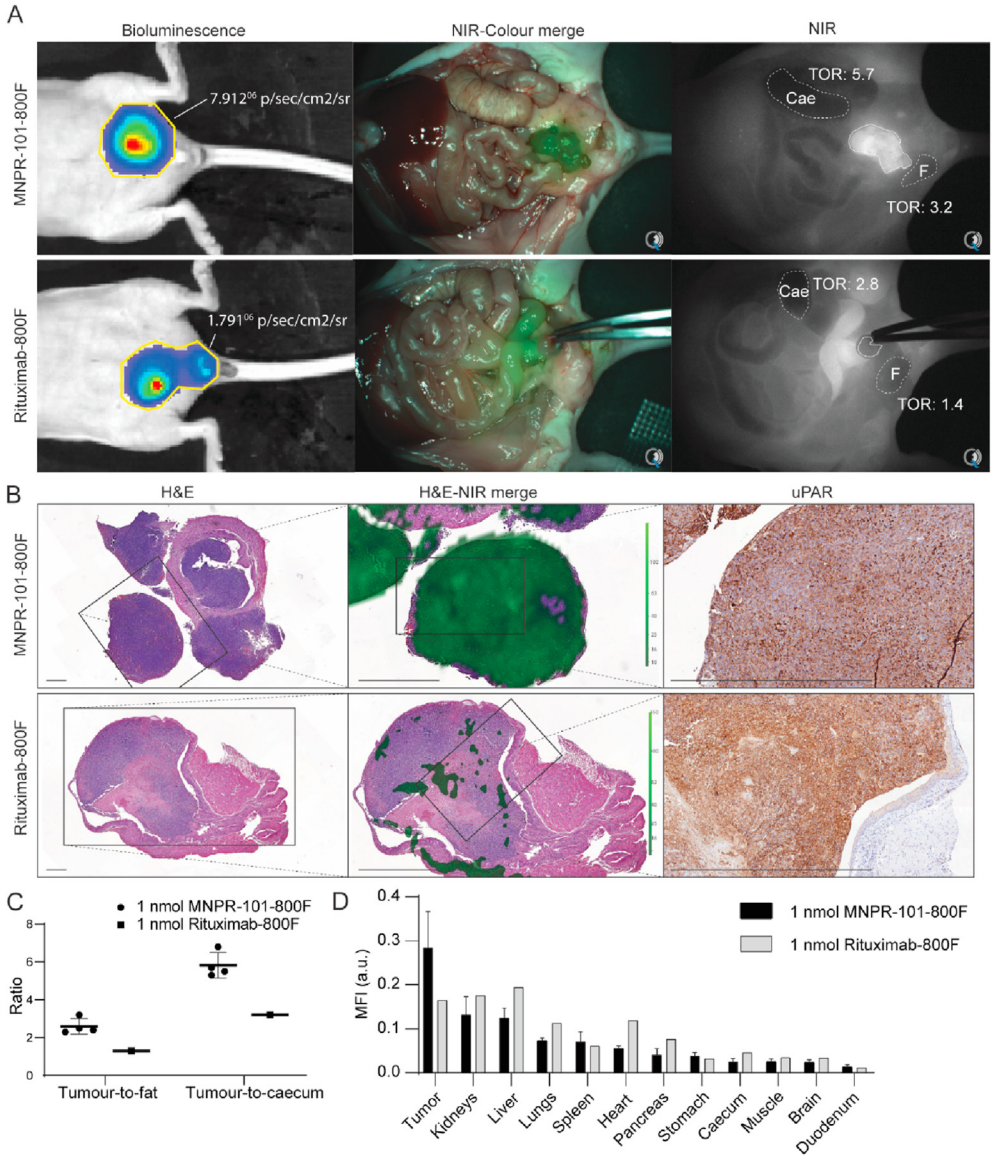

Fig. 4. uPAR NIR-guided surgery in a preclinical orthotopic UCC xenograft model. (A) Bioluminescence imaging and NIR image-guided resection with the clinical Artemis NIR camera three days after 1 nmol injection of MNPR-101-800F or rituximab-800F. (B) Post-mortem histological, fluorescence scanning (Odyssey) and uPAR immunolocalization of resected orthotopic tumours. (C) *In vivo* signal-to-background ratios measured during image-guided resection with the clinical Artemis NIR camera, and (D) post-mortem whole-body biodistribution determined using the Pearl. Cae, caecum; TOR, tumour-to-organ ratio; F, fat; UCC, urothelial cell carcinoma; NIR, near-infrared; uPAR, urokinase plasminogen activator receptor.

regarding penetration depth, tissue absorption, and scattering, and tissue autofluorescence and not adapted to most clinically used NIR imaging systems [23]. The favourable imaging characteristics of NIR-fluorophores pave the way for improved real-time NIR fluorescence guided resection of UCC.

To date, no single tracer is suitable for intraoperative guidance of all UCC specimens. As a result, a tracer library should be developed from which a surgeon can select the most suitable tracer [8]. Ideally, these tracers visualise unique characteristics of UCC which distinguishes the tumour from adjacent normal tissue. In case of uPAR and EpCAM, these membrane receptors have complementary expression patterns during the complex multistep process of switching from a sessile to an invasive cancer cell [24,25]. In addition to uPAR targeting, we show our recently introduced EpCAM-targeting tracer, which is currently being evaluated on patients with gastrointestinal cancer, could also be used for UCC (NL7363) [26]. Other potential combinations encompass epidermal growth factor receptor, human epidermal growth factor receptor 2 and/or matrix-metalloproteases, some of which are currently being investigated in clinical studies with other tumour types [8]. Release of these membrane proteins into the urine provide a possible surrogate biomarker for their respective tumour

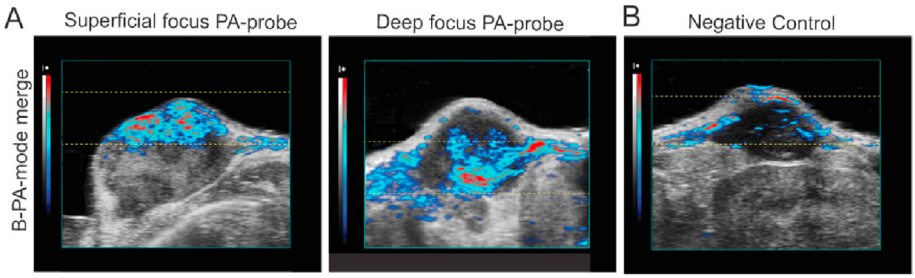

Fig. 5. Photoacoustic imaging of subcutaneously implanted UM-UC-3luc2 tumours *in vivo*. (A) MNPR-101-800F. (B) Negative control. Area between the yellow dotted lines represent the focus area of the photoacoustic probe. (For interpretation of the references to color in this figure legend, the reader is referred to the Web version of this article.)

expression and provides a simple non-invasive method for tracer selection. While both uPAR and EpCAM are elevated in urine from patients with UCC, the correlation with cellular expression has not yet been evaluated [27–30].

Although NIR-imaging has superior resolution, it is less suitable for imaging of lesions deeper than 1 cm [8]. PA, on the other hand, provides molecular contrast of up to 12-cm deep without compromising on the sub-millimetre spatial resolution. As a result, PA has been used for *in vivo* imaging of organelles to organs and has been incorporated in imaging platforms for transvaginal imaging of ovarian cancer and transrectal imaging of prostate cancer [31–33]. In the case of UCC, improved imaging depth allows the visualisation of deeper layers of the bladder, including the muscularis propria and peri-vesical fat, informing urologists of possible advanced T-stage disease during cystoscopy and the need of the more aggressive (partial) cystectomy [34,35].

We investigated whether NIR fluorescence-imaging could be performed in combination with PA, by using a contrast agent with a reasonable extinction coefficient and relatively low quantum yield (for PA-imaging a large non-fluorescence relaxation is desired), such as 800F ($\varepsilon = 2.4 \times 10^5$; $\Phi = 0.034$) [15]. In a proof-of-principle study, Tummers *et al.* [36] imaged pancreatic cancer *ex vivo* using both fluorescence and PA-imaging modalities. Similarly, the development of liver metastases *in vivo* was monitored bimodally using a single $\alpha_v\beta_3$ integrin targeting contrast agent, Angiostamp800 [37]. Our results show the feasibility of imaging through superficial structures such as the skin.

uPAR bimodal imaging is not limited to MNPR-101-800F. Its precursor, ATN-658, was previously dual-labelled for SPECT and NIR imaging using the hybrid ^{111}In and ZW800-1 label for imaging of locoregional oral and colorectal cancer. While procuring TBRs of 5.0 ± 1.3 and being able to visualise 1–2mm-sized lesions, the tracer is less suitable for PA imaging due to ZW800-1 quantum yield ($\varepsilon = 2.5 \times 10^5$; $\Phi = 0.150$) [13,14,38]. Another option is the uPAR targeting peptide AE105-Glu-Glu-ICG which has successfully identified multiple tumour types in various preclinical models with TBRs up to 3.5 ± 0.2 [39,40]. Its fluorophore, indocyanine green (ICG) has a similar extinction coefficient and quantum yield as 800F ($\varepsilon = 2.7 \times 10^5$; $\Phi = 0.027$) and has been used for previously for PA imaging [15]. Peptides generally clear rapidly from the circulation via the kidneys, which could be a limiting factor for bimodal imaging of UCC [41].

5. Conclusion

uPAR and EpCAM are complementary targets for NIR imaging of UCC that are indicative of separate tumour differentiation states. MNPR-101-800F targets uPAR and allows for simultaneous NIR and PA guidance. If confirmed in a clinical setting, such assistance can result in a paradigm shift, altering how urologists survey and treat UCC, thus potentially improving patient outcomes.

Ethics approval and consent to participate

The LUMC ethics review board approved the study protocol (B20.030). Samples and data were non-identifiable and used in accordance with the 1964 Helsinki declaration.

The Dutch Central Commission for Animal Experimentation approved all animal experiments (AVD1160020172925). Experiments were performed in accordance with the code of practice 'Dierproeven In Het Kankeronderzoek'.

Consent for publication

Not applicable.

Availability of data and materials

The data sets generated and/or analysed during the present study are available from the corresponding author on reasonable request.

Funding

C.F.M.S. and T.S. were in part funded by European Commission under two Marie Skłodowska-Curie Action awards: H2020-MSCA-RISE-2019 (Project number: 872860 - PRISAR2) and H2020-MSCA-ITN-2019 (Project number: 857894 - CAST).

G.v.d.H., M.H.v.d.M. and G.v.d.P. were partially funded by grants from the Dutch Cancer Society (EMCR 2015–8038, UL2014-7058).

Authors' contributions

The manuscript has been seen and approved by all authors. V.M.B., A.P.M., G.v.d.P., P.J.K.K., A.L.V. and C.F.M.S. were responsible for conception and design. V.M.B., G.v.d.H., M.M.D., S.S.B., T.S., V.Q.S., M.H.v.d.M., L.I. and H.d.J. acquired data. V.M.B., G.v.d.H., M.M.D., A.P.M., A.L.V. and C.F.M.S. analysed and interpreted data. V.M.B. and C.F.M.S. drafted the manuscript and performed the statistical analysis. A.P.M., G.v.d.P., A.L.V.H. and C.F.M.S. obtained funding. S.S.B., M.H.v.d.M. and M.R. performed important administrative, technical or material support. P.J.K., A.L.V. and C.F.M.S. supervised the project. All authors critically revised the manuscript for important intellectual content.

Conflict of interest statement

The authors declare the following financial interests/personal relationships which may be considered as potential competing interests

A.P.M. is a cofounder, employee and equity holder in Monopar Therapeutics. All other authors have no conflicts of interest to declare.

Acknowledgements

The authors would like to acknowledge N.G. Dekker-Ensink, R.L.P. Vlierberghe, M. Prevoo, R.D. Houvast, S.G. van Duinen (LUMC-Pathologie), R., Cordfunke and J. Overdevest (LUMC-Immunologie) and C.M. Jol-van der Zijde (LUMC-Willem-Alexander Kinderziekenhuis).

Appendix A. Supplementary data

Supplementary data to this article can be found online at https://doi.org/10.1016/j.ejca.2021.01.001.

References

[1] Bray F, Ferlay J, Soerjomataram I, Siegel RL, Torre LA, Jemal A. Global cancer statistics 2018: GLOBOCAN estimates of incidence and mortality worldwide for 36 cancers in 185 countries. CA Cancer J Clin 2018;68(6):394–424.

[2] Zehnder P, Studer UE, Skinner EC, Thalmann GN, Miranda G, Roth B, et al. Unaltered oncological outcomes of radical cystectomy with extended lymphadenectomy over three decades. BJU Int 2013;112(2):E51–8.

[3] Mitra AP, Jordà M, Cote RJ. Pathological possibilities and pitfalls in detecting aggressive bladder cancer. Curr Opin Urol 2012;22(5):397–404.

[4] Simon M, Bosset P-O, Rouanne M, Benhamou S, Radulescu C, Molinié V, et al. Multiple recurrences and risk of disease progression in patients with primary low-grade (TaG1) non-muscle-invasive bladder cancer and with low and intermediate EORTC-risk score. PloS One 2019;14(2):e0211721 [e].

[5] Kassouf W, Traboulsi SL, Schmitz-Dräger B, Palou J, Witjes JA, van Rhijn BWG, et al. Follow-up in non-muscle-invasive bladder cancer-International Bladder Cancer Network recommendations. Urol Oncol 2016;34(10):460–8.

[6] Novara G, Svatek RS, Karakiewicz PI, Skinner E, Ficarra V, Fradet Y, et al. Soft tissue surgical margin status is a powerful predictor of outcomes after radical cystectomy: a multicenter study of more than 4,400 patients. J Urol 2010;183(6):2165–70.

[7] Persson M, Skovgaard D, Brandt-Larsen M, Christensen C, Madsen J, Nielsen CH, et al. First-in-human uPAR PET: imaging of cancer aggressiveness. Theranostics 2015;5(12):1303–16.

[8] Hernot S, van Manen L, Debie P, Mieog JSD, Vahrmeijer AL. Latest developments in molecular tracers for fluorescence image-guided cancer surgery. Lancet Oncol 2019;20(7):e354–67.

[9] Spizzo G, Fong D, Wurm M, Ensinger C, Obrist P, Hofer C, et al. EpCAM expression in primary tumour tissues and metastases: an immunohistochemical analysis. J Clin Pathol 2011;64(5):415–20.

[11] Dohn LH, Pappot H, Iversen BR, Illemann M, Hoyer-Hansen G, Christensen IJ, et al. uPAR expression pattern in patients with urothelial carcinoma of the bladder–possible clinical implications. PloS One 2015;10(8):e0135824.

[12] Boonstra MC, Verspaget HW, Ganesh S, Kubben FJ, Vahrmeijer AL, van de Velde CJ, et al. Clinical applications of the urokinase receptor (uPAR) for cancer patients. Curr Pharmaceut Des 2011;17(19):1890–910.

[13] Boonstra MC, van Driel PB, van Willigen DM, Stammes MA, Prevoo HA, Tummers QR, et al. uPAR-targeted multimodal tracer for pre- and intraoperative imaging in cancer surgery. Oncotarget 2015;6(16):14260–73.

[14] Boonstra MC, Van Driel P, Keereweer S, Prevoo H, Stammes MA, Baart VM, et al. Preclinical uPAR-targeted multimodal imaging of locoregional oral cancer. Oral Oncol 2017;66:1–8.

[15] Weber J, Beard PC, Bohndiek SE. Contrast agents for molecular photoacoustic imaging. Nat Methods 2016;13(8):639–50.

[16] Vahrmeijer AL, Hutteman M, van der Vorst JR, van de Velde CJ, Frangioni JV. Image-guided cancer surgery using near-infrared fluorescence. Nat Rev Clin Oncol 2013;10(9):507–18.

[17] Baart VM, van Duijn C, van Egmond SL, Dijckmeester WA, Jansen JC, Vahrmeijer AL, et al. EGFR and αvβ6 as promising targets for molecular imaging of cutaneous and mucosal squamous cell carcinoma of the head and neck region. Cancers 2020;12(6).

[18] Xu X, Cai Y, Wei Y, Donate F, Juarez J, Parry G, et al. Identification of a new epitope in uPAR as a target for the cancer therapeutic monoclonal antibody ATN-658, a structural homolog of the uPAR binding integrin CD11b (alphaM). PloS One 2014;9(1):e85349.

[19] van der Horst G, van Asten JJ, Figdor A, van den Hoogen C, Cheung H, Bevers RF, et al. Real-time cancer cell tracking by bioluminescence in a preclinical model of human bladder cancer growth and metastasis. Eur Urol 2011;60(2):337–43.

[20] Leal J, Luengo-Fernandez R, Sullivan R, Witjes JA. Economic burden of bladder cancer across the European union. Eur Urol 2016;69(3):438–47.
[21] Dy GW, Gore JL, Forouzanfar MH, Naghavi M, Fitzmaurice C. Global burden of urologic cancers, 1990-2013. Eur Urol 2017; 71(3):437–46.
[22] Burger M, Grossman HB, Droller M, Schmidbauer J, Hermann G, Drăgoescu O, et al. Photodynamic diagnosis of non-muscle-invasive bladder cancer with hexaminolevulinate cystoscopy: a meta-analysis of detection and recurrence based on raw data. Eur Urol 2013;64(5):846–54.
[23] Gioux S, Choi HS, Frangioni JV. Image-guided surgery using invisible near-infrared light: fundamentals of clinical translation. Mol Imag 2010;9(5):237–55.
[24] Mahmood N, Mihalcioiu C, Rabbani SA. Multifaceted role of the urokinase-type plasminogen activator (uPA) and its receptor (uPAR): diagnostic, prognostic, and therapeutic applications. Front Oncol 2018;8:24.
[25] Nini A, Hoffmann MJ, Lampignano R, Grosse Siemer R, van Dalum G, Szarvas T, et al. Evaluation of HER2 expression in urothelial carcinoma cells as a biomarker for circulating tumor cells. Cytomet B Clin Cytom 2020 Jul;98(4):355–67. https://doi.org/10.1002/cyto.b.21877. Epub 2020 Mar 25.
[26] Boogerd LSF, Boonstra MC, Prevoo H, Handgraaf HJM, Kuppen PJK, van de Velde CJH, et al. Fluorescence-guided tumor detection with a novel anti-EpCAM targeted antibody fragment: preclinical validation. Surg Oncol 2019;28:1–8.
[27] Bryan RT, Shimwell NJ, Wei W, Devall AJ, Pirrie SJ, James ND, et al. Urinary EpCAM in urothelial bladder cancer patients: characterisation and evaluation of biomarker potential. Br J Canc 2014;110(3):679–85.
[28] Snell KIE, Ward DG, Gordon NS, Goldsmith JC, Sutton AJ, Patel P, et al. Exploring the roles of urinary HAI-1, EpCAM & EGFR in bladder cancer prognosis & risk stratification. Oncotarget 2018;9(38):25244–53.
[29] Casella R, Shariat SF, Monoski MA, Lerner SP. Urinary levels of urokinase-type plasminogen activator and its receptor in the detection of bladder carcinoma. Cancer 2002;95(12):2494–9.
[30] Shariat SF, Casella R, Monoski MA, Sulser T, Gasser TC, Lerner SP. The addition of urinary urokinase-type plasminogen activator to urinary nuclear matrix protein 22 and cytology improves the detection of bladder cancer. J Urol 2003;170(6 Pt 1): 2244–7.
[31] Wang LV, Hu S. Photoacoustic tomography: in vivo imaging from organelles to organs. Science 2012;335(6075):1458–62.
[32] Kumavor PD, Alqasemi U, Tavakoli B, Li H, Yang Y, Sun X, et al. Co-registered pulse-echo/photoacoustic transvaginal probe for real time imaging of ovarian tissue. J Biophot 2013;6(6–7): 475–84.
[33] Kothapalli SR, Sonn GA, Choe JW, Nikoozadeh A, Bhuyan A, Park KK, et al. Simultaneous transrectal ultrasound and photoacoustic human prostate imaging. Sci Transl Med 2019;11(507).
[34] Kamaya A, Vaithilingam S, Chung BI, Oralkan O, Khuri-Yakub BT. Photoacoustic imaging of the bladder: a pilot study. J Ultrasound Med 2013;32(7):1245–50.
[35] Liem EI, de Reijke TM. Can we improve transurethral resection of the bladder tumour for nonmuscle invasive bladder cancer? Curr Opin Urol 2017;27(2):149–55.
[36] Tummers WS, Miller SE, Teraphongphom NT, Gomez A, Steinberg I, Huland DM, et al. Intraoperative pancreatic cancer detection using tumor-specific multimodality molecular imaging. Ann Surg Oncol 2018;25(7):1880–8.
[37] Lavaud J, Henry M, Gayet P, Fertin A, Vollaire J, Usson Y, et al. Noninvasive monitoring of liver metastasis development via combined multispectral photoacoustic imaging and fluorescence diffuse optical tomography. Int J Biol Sci 2020;16(9):1616–28.
[38] de Valk KS, Handgraaf HJ, Deken MM, Sibinga Mulder BG, Valentijn AR, Terwisscha van Scheltinga AG, et al. A zwitterionic near-infrared fluorophore for real-time ureter identification during laparoscopic abdominopelvic surgery. Nat Commun 2019; 10(1):3118.
[39] Juhl K, Christensen A, Rubek N, Karnov KKS, von Buchwald C, Kjaer A. Improved surgical resection of metastatic pancreatic cancer using uPAR targeted in vivo fluorescent guidance: comparison with traditional white light surgery. Oncotarget 2019; 10(59):6308–16.
[40] Juhl K, Christensen A, Persson M, Ploug M, Kjaer A. Peptide-based optical uPAR imaging for surgery: in vivo testing of ICG-Glu-Glu-AE105. PloS One 2016;11(2):e0147428.
[41] Baart VM, Boonstra MC, Sier CFM. uPAR directed-imaging of head-and-neck cancer. Oncotarget 2017;8(13):20519–20.